Hindawi
Advances in Civil Engineering
Volume 2018, Article ID 8161498, 14 pages
https://doi.org/10.1155/2018/8161498

Research Article

A Mechanical Model of the Overlying Rock Masses in Undersea Coal Mining and a Stress-Seepage Coupling Numerical Simulation

Jie Fang,[1] Lei Tian,[2] Yanyan Cai,[3] Zhiguo Cao,[1] Jinhao Wen,[1] and Zhijie Wen[2,4]

[1]*State Key Laboratory of Coal Resources and Safe Mining, China University of Mining & Technology (Beijing), Beijing 100083, China*
[2]*State Key Laboratory of Mining Disaster Prevention and Control Co-Founded by Shandong Province and Ministry of Science and Technology, Shandong University of Science and Technology, Qingdao 266590, China*
[3]*Fujian Engineering Technology Research Center for Tunnel and Underground Space, Huaqiao University, Xiamen, Fujian 361021, China*
[4]*State Key Laboratory for Geomechanics and Deep Underground Engineering, China University of Mining and Technology (Beijing), Beijing 100083, China*

Correspondence should be addressed to Jinhao Wen; wenjh0532@163.com and Zhijie Wen; sdust0532@gmail.com

Received 19 January 2018; Accepted 18 July 2018; Published 12 September 2018

Academic Editor: Damien Rangeard

The water inrush of a working face is the main hidden danger to the safe mining of underwater coal seams. It is known that the development of water-flowing fractured zones in overlying strata is the basic path which causes water inrushes in working faces. In the engineering background of the underwater mining in the Longkou Mining Area, the analysis model and judgment method of crack propagation were created on the basis of the Mohr–Coulomb criterion. Fish language was used to couple the extension model into the FLAC^{3d} software, in order to simulate the mining process of the underwater coal seam, as well as to analyze the initiation evolutionary characteristics and seepage laws of the fractured zones in the overlying strata during the advancing processes of the working face. The results showed that, during the coal seam mining process, the mining fractured zones which had been caused by the compression-shear and tension-shear were mainly concentrated in the overlying strata of the working face. Also, the open-off cut and mining working face were the key sections of the water inrush in the rock mass. The condition of the water disaster was the formation of a water inrush channel. The possible water inrush channels in underwater coal mining are mainly composed of water-flowing fractured zones which are formed during the excavation processes. The numerical simulation results were validated through the practical engineering of field observations on the height of water-flowing fractured zone, which displayed a favorable adaptability.

1. Introduction

Mining activities under complicated conditions, especially underwater coal mining, have attracted constant attention recently, due to the increasing demand for coal resources. Underwater mining is a complex issue, which can be affected by mining activities. The fractures and failure instabilities of the surrounding rock masses within a mining space, especially the roof areas, are considered to be dynamic processes. Therefore, underwater mining activities should always give full consideration to the interactions between the ground stress, fractures, water, and so on [1–4]. The largest water masses in the world are in the sea. Furthermore, undersea mining technology also represents the highest level of underwater mining. The greatest concern of undersea coal mining is the prevention of the seawater flushing into the undersea coal mines. The undersea coal mine water inrushes are the major factors affecting the safety of undersea mining. According to some of the previous analyses, the water inrushes, which are caused by the development of

water-flowing fractured zones, and the connections with the overlying aquifers are the main reasons for water inrushes induced by roof caving [5–7]. Therefore, the examination of the damage height problems of the overlying strata in stopes should also be given appropriate attention [8–10].

The previous relevant research studies regarding coal mining under lakes, rivers, reservoirs, and aquifers which have been conducted in China have accumulated rich experience [11–13]. For example, using a physical test system of similar materials, Chen et al. [14] analyzed and discussed the laws and mechanisms of roof water inrushes during underwater mining processes. Also, in the engineering backgrounds of certain under-river coal mines, Lai et al. [15] used an indoor mechanical characteristic test experiment of roof rock masses, which included physical simulations, numerical simulations, and other means to consider the stress fields and overlying strata rupture instabilities as a dynamic system. Meanwhile, the field measurements and dynamic predictions of the stability laws of overlying strata and surfaces were conducted in order to provide guidance for the safe underwater production of this mine. Therefore, on this basis, a "three-zone" theory which was composed of a caving zone, water-flowing fractured zone, and overall mobile zone for the overlying strata failure was created and developed in China. An empirical formula was obtained, which used a fractional function for the prediction of the "three-zone" height, for the purpose of guiding the designs and practices of the underwater coal mining. Thereby, thick coal seam safety mining processes could be achieved under large surface water areas, such as the Huaihe River and Weishan Lake. These experiences have provided references for the technical and theoretical aspects, as well as the safety measures of undersea coal mining in China [16, 17].

In the engineering background of the underwater mining in the Longkou Mining Area, based on the above research, a FLAC^{3d} numerical model was established according to the specific geological conditions. Then, through the theoretical analysis of the roof structure mechanical model in this study, the roof movements and seepage laws during the process of the advancing working face were effectively simulated.

2. Criterion of Crack Propagation under Water Pressure

During the process of underwater coal mining, and under the coupling of seepage water pressure and coal seam mining, the roof rock beams of coal seams may become fractured, and fractured zones may form. Then, in accordance with the different rock mass failure patterns, the fractures can be divided into two categories. The first is when the rock masses already contained defective failure structures, such as large numbers of fissures. It is known that the failures of such structures are often derived from the opening of discontinuity and shear slip along the discontinuity. The other category is when new fractures are generated in the surrounding rock of the excavated rock masses, and the existing fractures propagate to the complete structure, which will eventually result in the destruction of the entire structure [18–20].

2.1. Water Pressure Calculation Method. The mechanical effects of groundwater on rock fractures are characterized by hydrostatic seepage pressure (p) and hydrodynamic pressure (tw) (surface force), of which the former tends to have expansion effects on the fractures. The distribution forces acting on the rock blocks include the transference of effective stress and seepage pressure (p). Coal seams, along with their upper and lower strata, belong to sedimentary rock. When the water inrushes of a working face are not formed, the fissure water will not be active, and the hydrostatic seepage pressure (p) in the rock masses plays a leading role [21]. The seepage hydraulic pressure in rock masses can be calculated as follows:

$$p = \gamma (H - z), \tag{1}$$

where γ is the unit weight of seepage fluid (kN/m^3), H denotes the distribution along the fracture water head (m), and z is the position height (m). The mechanical effects of seepage on the stress field of the rock masses are macroscopically the seepage body force of the dynamic change, which can be determined by the analysis of the seepage field. When calculating the deformation of rock masses, the total stress should be used, and the effective stress should be applied when calculating the deformation of a fracture system [22].

2.2. Criterion of Preexisting Fracture Cracking. The stabilities and failures of massive fracture structures are traditionally analyzed using the Mohr–Coulomb failure criterion. The existing discontinuities, such as the fractures and interfaces of different materials, have three forms as follows: a complete closure cementing state, a closed state, and opening state after failures. Under the influence of seepage pressure, and based on the Griffith criterion, the effective stress was applied to the Mohr–Coulomb criterion in the state of compression-shear as follows:

$$\sigma_1 - p = \sigma_c + q(\sigma_3 - p), \tag{2}$$

where σ_c represents the rock uniaxial compressive strength (MPa) and $q = \tan^2\alpha = (\sqrt{\tan^2\varphi + 1} + \tan\varphi)^2$ (MPa). Among these, α denotes the angle between normal fracture surface and the first principal stress direction (°) and φ is the internal friction angle of the rock mass (°).

The minimum normal stress was tested under the seepage pressure, $\sigma_3' = \sigma_3 - p$. When p increased to $p > \sigma_3$, $\sigma_3' < 0$, it became tensile stress. When $\sigma_3' = -T_0$ ($-T_0$ representing the tensile strength of the rock medium), tensile ruptures will occur in rock masses [23, 24].

There are obvious differences observed in the generation and propagation mechanisms during the state of tension-compression. The Mohr–Coulomb criterion is a statistical structure which has the ability to describe the common roles of massive fracture activities in shear rock failures. Meanwhile, the Griffith theory analytically describes single fracture behavior. Both of these have different methods and angles.

However, they are able to obtain the same results, which have been observed to have profound physical significance.

2.3. Criterion of the New Fracture Propagations. The local propagations of new fractures are characterized by stress concentrations. Under hydraulic actions, splitting occurs, which often reflects that the overall structures are unable to achieve the yield or failure conditions. Meanwhile, stress concentration phenomena have taken place in the local structures, which have led to material damages. Meanwhile, stress concentrations continue to occur along the failure areas, which will result in the propagation of the fractures.

The splitting caused by the water pressure is different from that which is caused by other mechanical effects. Due to water's liquidity, when new fractures appear, they will be immediately filled with water, and water pressure will be transferred to the fracture surfaces. Then, under the actions of the tension force, the fractures are considered to be type I. In the application of the classical Griffith theory, it is assumed that, for the rock fractures with maximum lengths of 2a, the fracture surface will be under the effective tension of $\sigma_3' = -T_0$ (MPa), and stress intensity factor will be as follows:

$$K_1 = Y\left|\sigma_3'\right|\sqrt{\pi a}, \tag{3}$$

where K_1 represents the stress intensity factor (MPa·m$^{1/2}$) and Y is the geometric correction factor. When $K_1 = K_{1C} = Y = Y|\sigma_3'|\sqrt{\pi a}$, the fractures will begin to propagate. If the fracture fluids are constantly replenished through seepage, the fracture pressure will be maintained, which will continue the propagation process in this part of the fractures [25–27].

3. Criterion of the Fracture Propagation

From the perspective of the energy for the analyses, the fractures of the rock material were found to be mainly due to external factors rather than the value of the material itself, in which case the rock material will begin to become damaged. Therefore, the more energy the material itself undertakes, the greater the extent of the damage will be. In the original fracture, the fracture tip was observed to be not very sharp. Therefore, the energy accumulation was not high, and the splitting was slow. Then, following the splitting, the fracture tip became very sharp, and a great deal of energy was gathered, which led to rapid constant splitting of the rock fractures [18, 20, 23–25]. Therefore, the angle of the energy was determined to be a suitable method for judging the fracture splitting degree.

Following the rock damage, due to the microstructure changes, the material strength became lower, and the seepage ability was stronger. Therefore, the damage variable D was added in this study for the damage degree criterion of the unit. The damage degree of the rock mass was determined according to the ratio of the unit dissipation energy and the critical strain energy of the rock mass [28]. The strain energy of the rock unit was determined as follows:

$$\frac{dW}{dV} = \int_0^{\varepsilon_{ij}} \sigma_{ij} d\varepsilon_{ij}. \tag{4}$$

In this study, based on the judgment criterion of this energy, the Fish function of FLAC^{3d} was used to judge the fracture splitting. Figure 1 details the looping of the Fish language program for the fissure propagation [29].

In order to facilitate the calculation, this study ascertained that the stress-strain curve of the rock mass could be simplified into a bilinear stress-strain model, which was composed of two lines, as shown in Figure 2. Therefore, the area which was enveloped by the stress-strain curve was considered to be the tolerated energy for the unit. The external force applied on unit was partially used for increasing the elastic energy of the material, as well as partially changing the unit shape, and was consumed by other types of energy, such as sound waves and fracture propagation. This is theoretically known as the dissipative strain energy density of a unit as follows:

$$\left(\frac{dw}{dv}\right)_d = \left(\frac{dw}{dv}\right) - \frac{1}{2E_0^*}\left(\sigma_1^2 + \sigma_2^2 + \sigma_3^2 - 2v\left(\sigma_1\sigma_2 + \sigma_2\sigma_3 + \sigma_3\sigma_1\right)\right). \tag{5}$$

The sum of the dissipative energy of a unit during a single loading process is S_{uaf}, where E_0^* is Young's modulus after the deduction, which is related to the previous stress path. It is known that when the energy of a unit is greater than the maximum elastic energy, fractures will begin to appear. The directions of the fractures will be generally in the direction of σ_3, or alternatively, in the direction of the maximum tensile stress.

At the beginning of this experimental study, the strain energy density of the unit was set to 0 (z_extral = 0). When the calculation reached the ith step, the strain energy density of the unit could be obtained as follows:

$$\begin{aligned}\left(\frac{dW}{dV}\right)_i = {} & \left(\frac{dW}{dv}\right)_{(i-1)} + \frac{1}{2}\left(\sigma_x^i + \sigma_x^{i-1}\right)\left(\varepsilon_x^i - \varepsilon_x^{i-1}\right) \\ & + \frac{1}{2}\left(\sigma_y^i + \sigma_y^{i-1}\right)\left(\varepsilon_y^i - \varepsilon_y^{i-1}\right) + \frac{1}{2}\left(\sigma_z^i + \sigma_z^{i-1}\right)\left(\varepsilon_z^i - \varepsilon_z^{i-1}\right) \\ & + \frac{1}{2}\left(\sigma_{xy}^i + \sigma_{xy}^{i-1}\right)\left(\varepsilon_{xy}^i - \varepsilon_{xy}^{i-1}\right) \\ & + \frac{1}{2}\left(\sigma_{yz}^i + \sigma_{yz}^{i-1}\right)\left(\varepsilon_{yz}^i - \varepsilon_{yz}^{i-1}\right) \\ & + \frac{1}{2}\left(\sigma_{yz}^i + \sigma_{yz}^{i-1}\right)\left(\varepsilon_{yz}^i - \varepsilon_{yz}^{i-1}\right).\end{aligned} \tag{6}$$

The strain energy accumulation of the unit in the simulation process was recorded, where σ_x^i, σ_y^i, σ_z^i, σ_{xy}^i, σ_{yz}^i, and σ_{xz}^i represent the unit stresses of the ith step. Meanwhile, σ_x^{i-1}, σ_y^{i-1}, σ_z^{i-1}, σ_{xy}^{i-1}, σ_{yz}^{i-1}, and σ_{xz}^{i-1} denote the unit stresses of the previous step, and the same expression was used for strain.

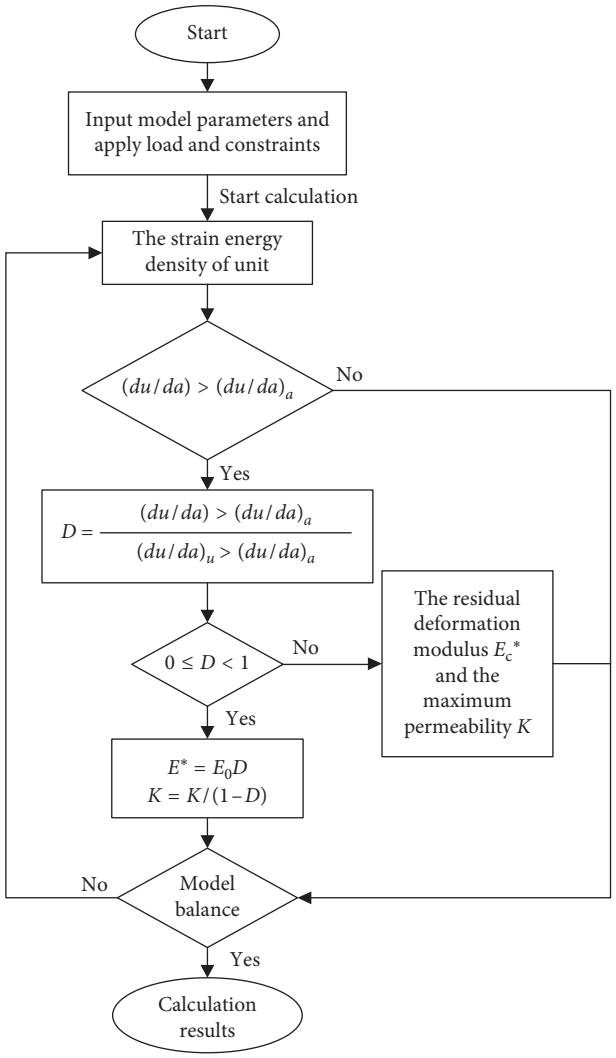

Figure 1: Flow chart of the numerical simulation.

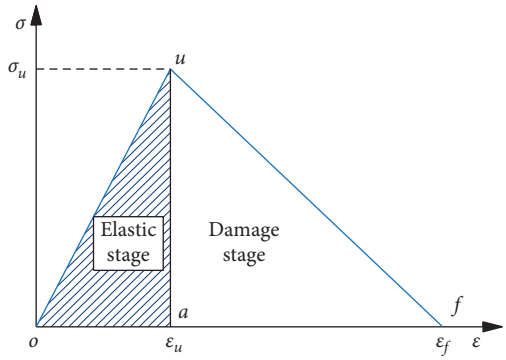

Figure 2: Bilinear stress-strain curve.

(i) When the energy (dW/dV) contained in the unit was $(dW/dV) \le S_{oua}$, where S_{oua} is the elastic energy density, recorded as $(dw/dv)_a$, the unit was determined to not be damaged.

(ii) When the energy contained in the unit was $S_{oua} < (dW/dV) < S_{ouf}$, where S_{ouf} is the maximum strain energy density of the unit, recorded as $(dw/d)_u$, the damage variable D was defined according to the ratio of (dW/dV) and S_{ouf}.

(iii) When $(dW/dV) > S_{ouf}$, it was considered that the unit had been of complete failure to lose its bearing capacity. Meanwhile, in order to ensure no singularity for the unit, the unit was given by a residual volume modulus K^* and the greater permeability k^*.

It should be pointed out that the unit which had lost its bearing capacity was unable to represent the structural failures. With the triaxial compression, although the material had lost the cohesive force, the structural failures did not occur. Furthermore, the rock damages appeared only when the confining pressure was removed. Therefore, it was found to be very practical to give a small volume variable and a relatively large permeability, to the damage unit.

Therefore, more accurate numerical simulations could be conducted on the damage conditions of the surrounding rock masses and the development of the water-flowing fractured zones during the mining processes.

4. Rock Mass Seepage Mechanism Based on a Stress-Seepage Coupling Model of the Fractured Mining Rock Masses

During the mining processes, the underground coal resources are stoped to form goafs. The changes in the original stress states result in the formations of strata subsidence, displacement, and deformation. In the usual cases, three zones will be formed in the vertical direction due to the effects of gravity. These include caving zones, fractured zones, and bending zones. The caving zones are the collapse zones above the goafs, where obvious bed separations and displacements have occurred in the rock masses under self-gravity conditions. The fractured zones are located above the caving zones, where a large number of strong and visible cracks and fractures have occurred inside the rock masses. Finally, the bending zones are located above the fractured zones, where no structural failures have yet occurred to the rock masses. The interiors of these zones are affected by elastic deformations and will display downward bending trends. During large underwater coal mining operations, the opening of discontinuity on the roofs of the coal seams, along with the shear slip along the discontinuity, will become aggravated under the coupling of the seepage water pressure and the coal seam mining processes [30–32].

4.1. Mechanical Structure Model of the Heights of the Water-Flowing Fractured Zones. As detailed in Figure 3, in accordance with the advancing movement characteristics of the undersea coal seam mining field, a structure model of the mining field was established in this study [33–36].

The overlying strata damages which were caused by mining processes were considered to be a very complicated physio-omechanical phenomenon. A large number of observations indicated that the damage degrees of the overlying strata in the goaf could be divided into three zones as follows: a caving zone, fractured zone, and bending zone, as shown in Figure 3.

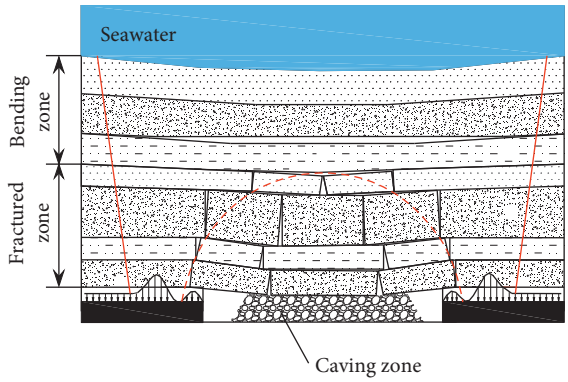

Figure 3: A structure model of the mining field.

4.1.1. Caving Zone. The rock mass after the rupture displayed the characteristics of an irregular collapse, in which the arrangement was also extremely irregular. The loose coefficient was relatively large, generally reaching between 1.3 and 1.5. However, after the recompaction, the broken expanding coefficient reached approximately 1.03. This zone was adjacent to the roof of the mining area and was directly formed by the immediate roof caving in most cases.

4.1.2. Fractured Zone. The fractured zone refers to the area with a rock block still arranged neatly following a rock rupture and is located above the caving zone. Due to this area's orderly arrangement, the broken expanding coefficient was small. The broken blocks of key strata were able to form the structure of a "voussoir beam."

4.1.3. Bending Zone. All of the strata from the top of the fractured zone to the surface are referred to as the bending zone. In the bending zone, the distinctive features of the strata movement are the continuity and integrity of the strata movement process. For example, the movement of the stratum from the top of the fractured zone to the surface occurs with stratification and integrity. In the vertical profile, the subsidence values of the upper and lower parts appear to be very small. If a key stratum exists in a thick and hard state, a bed separation zone may occur in the bending zone.

4.1.4. Water-Flowing Fractured Zone. A water-flowing fractured zone is the general term for the caving and fractured zones. For example, it refers to an overlying stratum aquifer located within the "two-zone" range, which leads to the rock water flowing into the goaf and stoped working face through rock fractured fissures.

The height and lithology of the water-flowing fractured zone are related to the mining height. The harder the overlying stratum is, the greater the height of the water-flowing fractured zone will be. Generally speaking, the height of the soft rock will be 9 to 12 times that of the mining height; that of the medium to hard rock will be 12 to 18 times; and that of hard rock will be 18 to 28 times.

4.2. Rock Seepage Characteristics Based on the Stress-Seepage Coupling Model of the Fractured Rock Mining Mass. The rock masses are generated by the cutting of massive fractures with random distributions. The existence of these fractures forms important channels for groundwater flow in rock masses. Due to the changes in original stresses following coal seam mining, increased stress zones and decreased stress zones occur in the surrounding rock of the coal seams. These changes lead to a series of mechanical effects on the overlying stratum of the coal seams, such as caving, fractures, bed separations, deformations, and displacements. When aquifers and water occur in the surrounding rock of coal seams, due to the influences of the mining processes, the occurrence states of the aquifers themselves will be affected, resulting in different mechanical characteristics. Meanwhile, the aquicludes at the roofs and floors of the aquifers will be impacted by the mining processes. Water-conductive channels may possibly be formed, which will change the hydraulic characteristics of the surrounding rock masses.

4.2.1. Establishment of the Numerical Model. In this study, the coal seam had a thickness of 4.4 m and was buried at a depth of 350 m. The working face had an inclined length of 150 m and a simulated advancing length of 200 m. In order to eliminate the boundary effects, based on a boundary with a width of 150 m, the strata with similar lithology were merged in a vertical direction, and the rock thickness was taken from the actual thickness. Then, through simulations up to the surface, the simplified model was 500 m long and 450 m wide, with a vertical height of 365 m. In accordance with an initial water level elevation of −96 m for the drilling process, the water head pressure was approximately 2.5 MPa. Meanwhile, improvements were made to the saving unit and operational speed, and the unit density was adjusted according to regional emphasis in order to ensure the precision of the calculation. Figure 4 details the model hierarchical schematic diagram, as well as and numerical model.

The mechanical boundary conditions of the model for the calculation were determined as follows: (1) A horizontal restraint was applied to the front-rear and left-right boundaries of the model. For example, the boundary horizontal displacement was set as zero; (2) the bottom boundary of the model was fixed. For example, the horizontal displacement and vertical displacement of the bottom boundary were set as zero; and (3) the top of the model was the free boundary area. Parameters of coal and rock are shown in Table 1.

An equivalent load was applied to the top of the model (geostatic stress). The load $\sigma_X = \sigma_Y = \lambda\sigma_Z$ was obtained by the following equation:

$$\sigma_Z = \gamma H, \tag{7}$$

where γ represents the volume force of the overlying strata (27 kN/m^3) and H is the depth from the top of the model to surface (m).

The lateral stress generated by the geostatic stress was imposed in the horizontal direction and is determined by the following equation:

$$\sigma_X = \sigma_Y = \lambda\sigma_Z, \tag{8}$$

where γ is the lateral pressure coefficient, which was determined by $\gamma = \mu/(1-\mu)$, in which μ is Poisson's ratio.

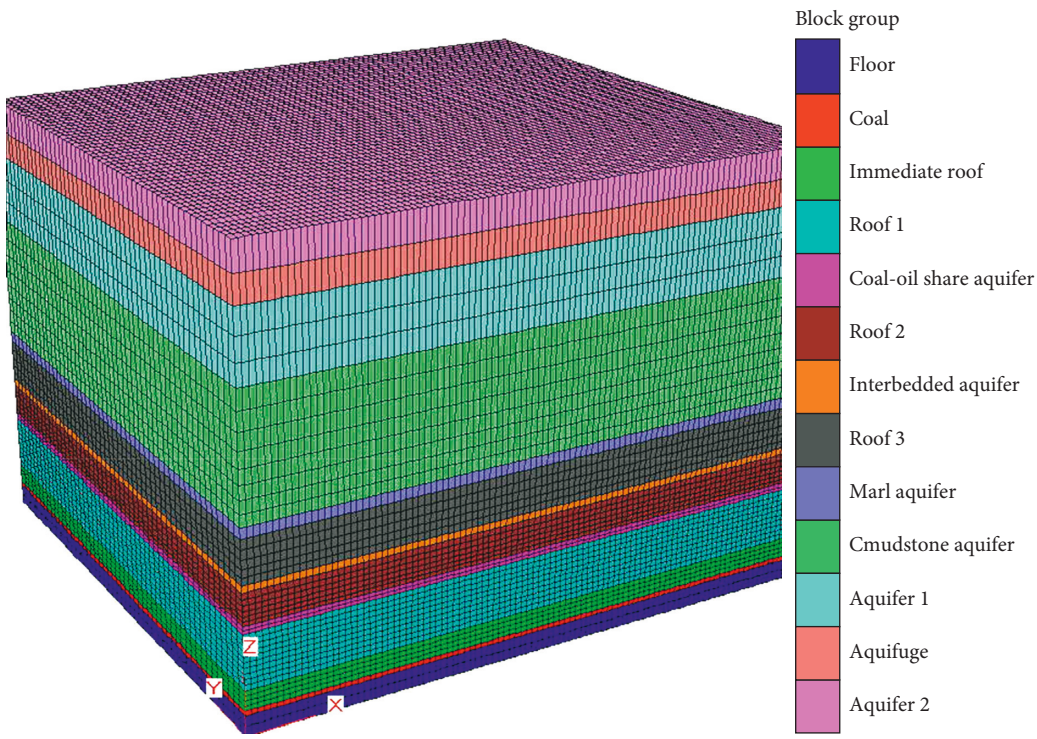

Figure 4: 3D model map.

Table 1: Parameters of coal and rock.

Lithology	Density (kg/m^3)	Elastic modulus (MPa)	Poisson's ratio	Internal friction angle (°)	Cohesion (MPa)	Tensile strength (MPa)
Aquifer 2	2.00	10	0.31	34.6	0.13	0.002
Aquifuge	2.01	160	0.28	33.4	0.71	0.11
Aquifer 1	2.02	2300	0.24	32.3	0.92	0.21
Cmudstone aquifer	2.30	1400	0.13	36.7	1.71	0.67
Marl aquifer	2.00	1200	0.21	30.4	1.42	0.89
Roof 3	2.60	75	0.13	36.1	0.33	0.08
Interbedded aquifer	2.50	1000	0.30	28.5	1.71	0.76
Roof 2	1.80	800	0.16	37.8	1.62	0.48
Coal-oil shale aquifer	1.80	900	0.28	40.4	2.10	0.55
Roof 1	2.02	200	0.35	26.2	0.32	0.02
Immediate roof	1.80	350	0.26	26.7	2.01	0.42
Coal	1.50	40	0.34	29.6	0.51	0.45
Floor	2.40	1900	0.32	33.1	2.10	1.52

An impermeable boundary was obtained around the model, and the excavated section was considered as the drainage boundary. The initial pore water pressures were given to the left and right boundaries of the model. The pore water pressure corresponded to the different water level conditions, in accordance with the linear changes in the hydraulic gradient.

4.2.2. Results of the Analysis of the Numerical Simulation

(1) Vertical Stress Contour. Figure 5 shows the simulation results of the vertical stress field when the working face had advanced 120 m along the strike. The coal stress variation in front of the coal wall reflected the caving changes of the top of the coal roof above the working face. It could be seen from the analysis that when the working face had advanced 16 m, the coal stress peak in front of the coal wall had changed greatly for the first time. Therefore, it was determined that the first caving occurred on the immediate roof of the working face. When the working face had advanced 36 m, the coal stress peak had greatly changed for a second time. Thereby, it was determined that the initial caving had occurred to the basic roof of the working face at that point. When the working face had advanced 54 m, a third major change was observed in the coal stress peak, and at that

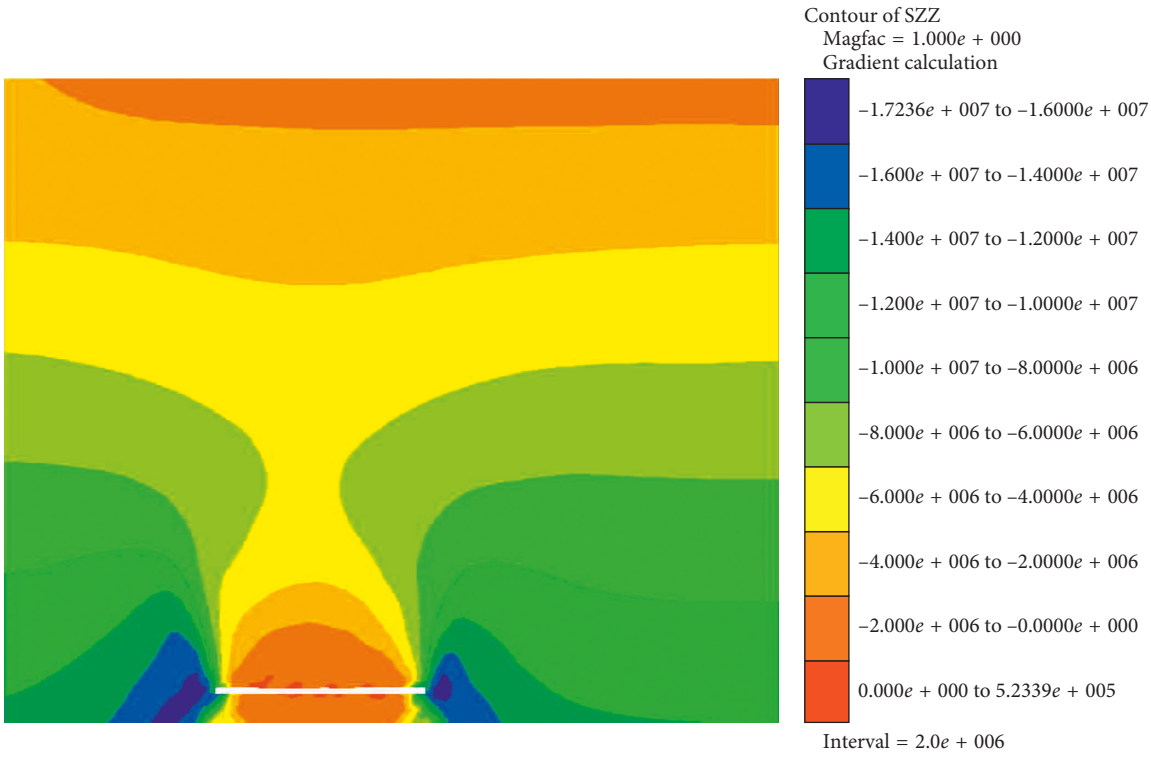

Figure 5: Vertical stress field when the working face had advanced 120 m.

point, the first periodic caving occurred to the basic roof of the working face. When the working face had advanced 72 m, the coal stress peak displayed major changes for the fourth time. At that point, the second periodic caving occurred to the basic roof of the working face. When the working face had advanced 84 m, there was a fifth major change in the coal stress peak, and the third periodic caving occurred to the basic roof of the working face. When the working face had advanced 98 m, the coal stress peak experience a major change for the sixth time, and the fourth periodic caving occurred to the basic roof of the working face. Finally, when the working face had advanced 120 m, the coal stress peak displayed a major change for the seventh time (Figure 6(a)), and the fifth periodic caving occurred to the basic roof of the working face. Meanwhile, stress reduction zone was produced on the roof and floor, and certain stress concentrations were generated in front of the coal wall, as well as behind the mine's working face.

As the working face continuously advanced, the roof pressure above the goaf changed minimally and the increase of the stress reduction zone in height gradually slowed down, which eventually tended to be stabilized to about 38 (m). The change of stress reduction zone in height of overlying strata is shown in Figure 6(b). Meanwhile, the abutment pressure in front of the working face moved continuously forward with the constant advancements of the mine and formed the lead abutment pressure. This could be divided into three areas as follows: the undisturbed zone of the mine, affected zone of the mine, and seriously affected area of the mine.

(2) Distribution Characteristics of the Failure Field. In this study, through the analysis of the failure field, the area after the failure of roof strata, which was posterior to the mining of the working face, could be intuitively presented. It could be seen that the distribution of the plastic zone above the front and rear coal walls of the goaf, and the area of the goaf, basically corresponded to the development ranges of the caving and fractured zones. It was observed that, from the bottom to the top of the coal seam roof, the tensile failure zone, tensile fracture zone, shear failure zone, and undamaged zone had become successively developed. The specific zones are shown in Figure 7. Among these, the tensile failure zone referred to the area where the strata were pulled and collapsed under the action of bidirectional tensile stress. In the tensile fracture zone, since the tensile stress in a certain direction exceeded the tensile strength of the rock mass, tension fractures were produced in a certain direction, of which the widths and connections differed with the various seepage abilities and failure degrees of the rock mass. Both of these regions were mainly distributed in the strata of the tensile stress zone above the goaf. Therefore, it was concluded that the roof failure of the working face was first of all a shear failure, which had led to the development of roof fractures. This was followed by tensile failure, which eventually resulted in breakage and caving. Therefore, the caving of the immediate roof was the result of tensile failure, and the development heights of the caving and fractured zones could be determined by the ranges of the tensile failures and the tensile fracture zones.

Figure 8(a) shows the distribution of the failure field on coal seam roof when the working face had advanced 120 m. It was confirmed from the analysis of the failure field that when the working face advanced 40 m, shortly after the first

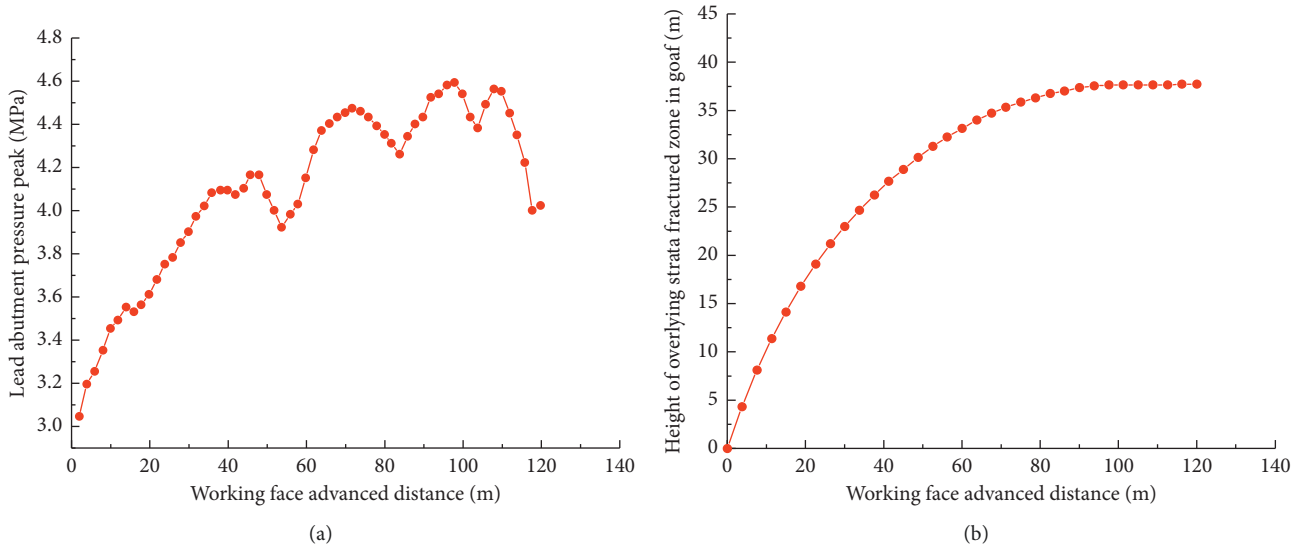

Figure 6: Numerical simulation curve of stress field. (a) Peak change curve of the lead abutment pressure of the working face. (b) Height of overlying strata fractured zone in goaf.

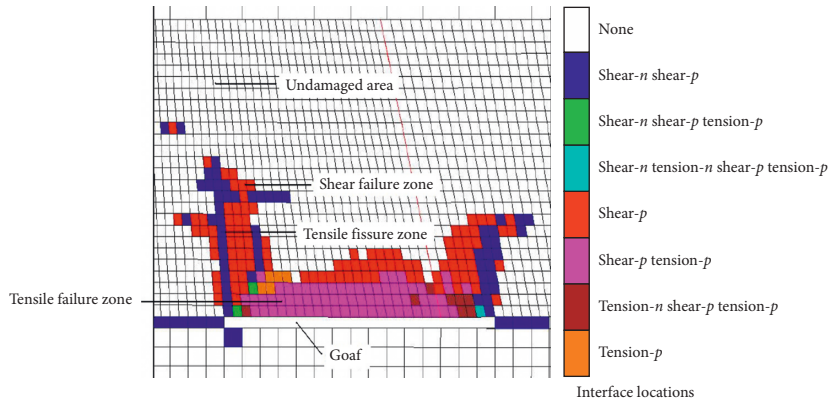

Figure 7: Failure field zoning.

caving of the basic roof, a caving angle of approximately 45° occurred to the immediate roof, and full caving had not yet occurred. When the working face advanced 80 m, there were no significant changes in the roof caving and immediate roof caving, when compared with previous situations near the time of the third periodic caving of the working face. The failure height of the overlying strata was observed to be developed upwards, with the advancement of the working surface. When the working face advanced approximately 120 m, the failure of the overlying strata had partially affected the $coal_1$-oil_2 aquifer.

With the continuous advancement of the working face, the increase of the failure field in height gradually slowed down and finally stabilized at around 39 m. The change of failure field in height of overlying strata is shown in Figure 8(b). It was obtained through the analysis performed in this study that, due to the open-off cut stoping of the working face, obvious damage areas had been generated on the roof and floor of the working face, as well as the front and rear areas of the coal wall. From the bottom to the top of the coal seam roof, tensile and shear failures had developed in turn.

(3) Distribution Characteristics of the Pore Water Pressure. The existence of pore pressure changed the constitutive characteristics of the fractured rock mass and thereby influenced the deformations. The changes in the pore water pressure and gradient distribution were found to directly affect the stress-strain relationship of the rock mass.

Figures 9–12 show the distribution changes of the pore water pressure during the process of the working face advancement. It can be seen from figures that, with the advancement of the working face, tensile and plastic changes first occurred to the open-off cut and coal wall support end. The fractures were generated with space extending, resulting in improvements in the permeability, and the pore water pressure became increased. With the advancement of the working face, the overlying strata at the center of the goaf became compacted, and the fractures were closed. Therefore,

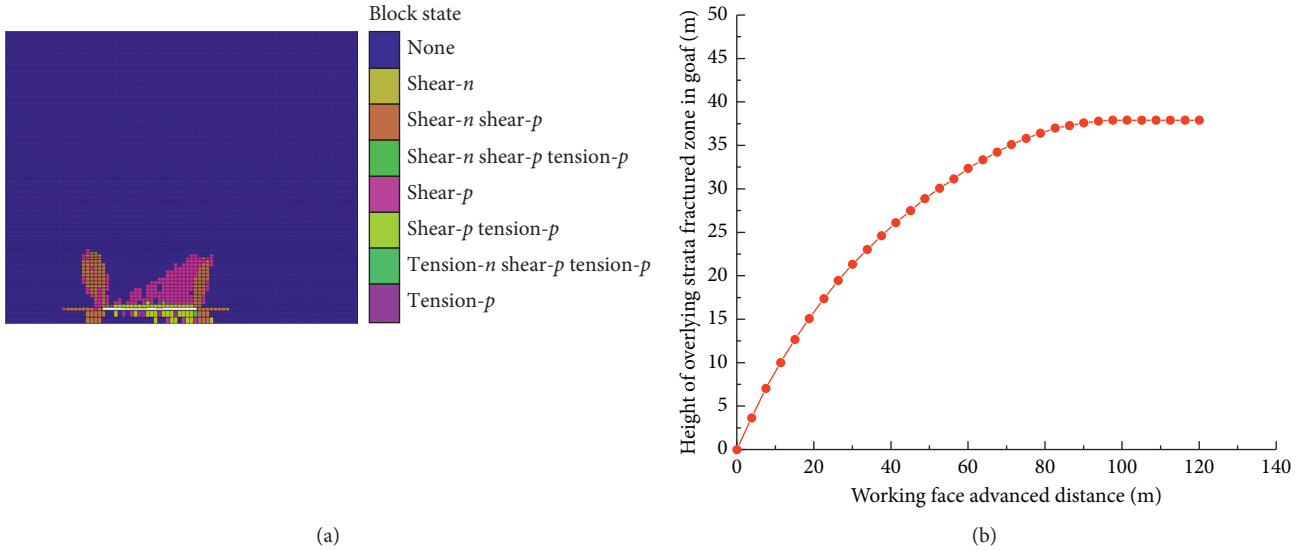

Figure 8: Numerical simulation curve of failure field. (a) Failure field when the working face had advanced 120 m. (b) Height of overlying strata fractured zone in goaf.

the permeability decreased, and the hydraulic gradient increased, while the pore pressure declined. Once the fractures were completely closed, the pore pressure disappeared. Also, due to the advancement of the working face, the roof failure height increased and gradually reached the overlying aquifer, which resulted in the water level of the aquifer dropping. This formed a descending funnel, with the goaf as the center.

(4) Flow Vector Diagram. Figures 13–19 reflect the overlying strata failure and the aquifer water flow vector characteristics in the cases of different time steps for the various advancing lengths during the process of the working face advancement. The rock fracture development and connections, as well as the water inrush processes and locations, under the conditions of the advancement of the mine, could then be intuitively obtained.

As working face advanced, failures first occurred to the open-off cut and coal walls. The disturbances caused by mining processes tend to destroy the original rock stress state, which then leads to the redistribution of the surrounding goaf stress. Therefore, the water route status of the roof aquifer first changed and presented a flow state towards the goaf, as detailed in Figures 13 and 14.

With the advancement of the working face, the failure depth of the overlying strata developed upwards. It was observed that, around the open-off cut and in front of the coal wall support, the water-flowing fractured zone was first connected with the aquifer to form a water-conductive channel. At the center of the goaf, the overlying strata showed a lower failure development. However, with the advancement of the working face, the rear goaf gradually showed a state of compaction, and water inrushes occurred at the front of the coal wall, as shown in Figures 15–19.

As viewed from the simulation results of the overlying strata failure, and the aquifer water seepage process caused by the coal seam mining, the roof caving and fracturing due to the mining processes had spread to overlying aquifer. Therefore, with the fractured zone now connected with the aquifer, the aquifer water infiltrated to the goaf, which led to water inrushes.

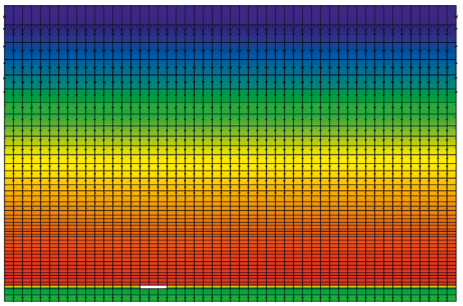

Figure 9: Distribution of the pore water pressure when the working face had advanced 30 m.

5. Field Observations of the Height of the Water-Flowing Fractured Zone. In this experimental study, by applying an "underground upward inclined drilling height-measuring instrument," upward inclined holes were drilled in the water-flowing fractured zone above the goaf and near the working face. Meanwhile, a double-head water-stopped machine was used to observe the height of the water-flowing fractured zone of the coal mining face under the Beizao Mine. The purpose was to analyze the overlying strata deformation and failure laws of the marine mining face and to provide scientific technical parameters for smooth and safe undersea mining operations [37].

The method involving ground borehole flushing fluid loss observations is known to be one of the most reliable traditional methods. However, for mining under large water

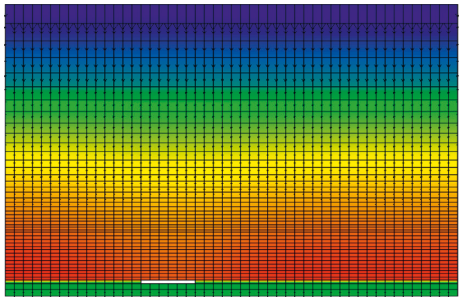

Figure 10: Distribution of the pore water pressure when the working face had advanced 60 m.

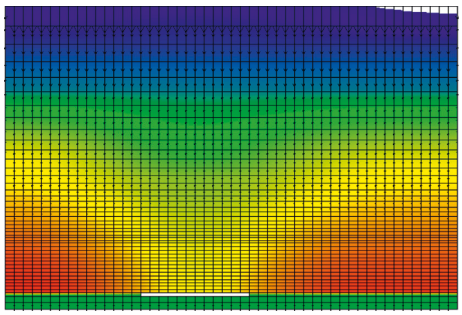

Figure 11: Distribution of the pore water pressure when the working face had advanced 120 m.

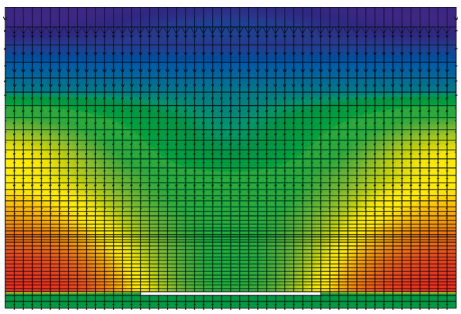

Figure 12: Distribution of the pore water pressure when the working face had advanced 140 m.

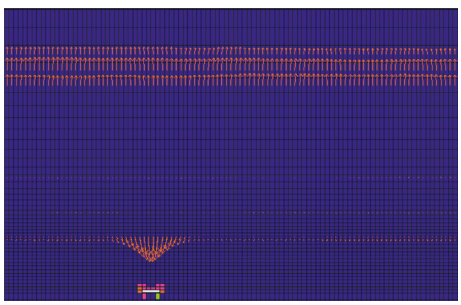

Figure 13: Flow vector diagram when the working face had advanced 20 m.

masses, due to water covering the surfaces, the traditional method for observing the height of water-flowing fractured zone using ground drilling has been found to be impossible

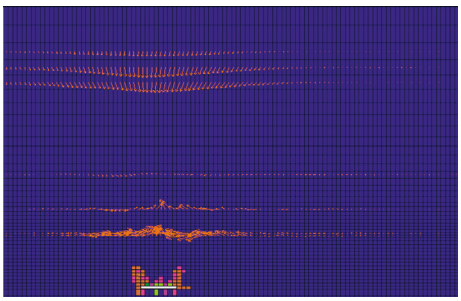

Figure 14: Flow vector diagram when the working face had advanced 40 m.

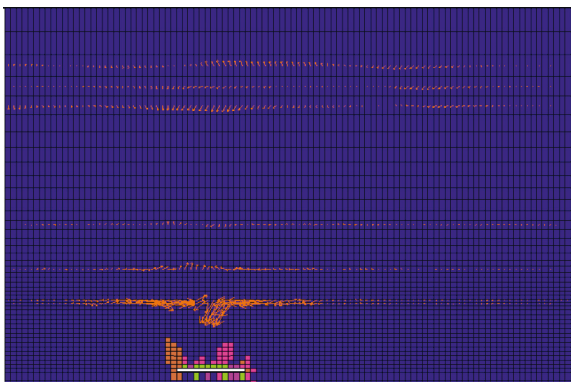

Figure 15: Flow vector diagram when the working face had advanced 60 m.

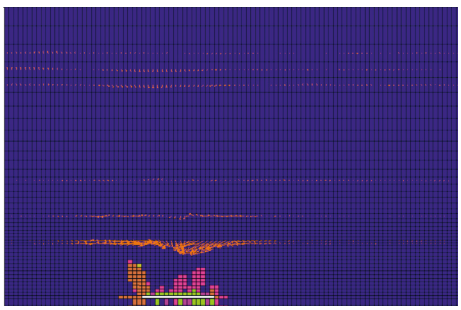

Figure 16: Flow vector diagram when the working face had advanced 80 m.

to implement. In this study, a method of underground uphole water injection for measuring loss was applied. For example, upward inclined holes were drilled above the goaf in the proper position of the coal mining face, which passed through the water-flowing fractured zone and entered the bending zone with the length of 10 m above the zone below (about 10 m), as shown in Figure 20. By using a height-measuring instrument, the water conductivity of rock strata was tested from the orifice to the bottom of the borehole in the measured length of 1 m. Then, according to the seepage situations of the boreholes at different depths, the height of the water-flowing fractured zone was determined.

In this study, based on the existing layout of the roadways, a height observation station was chosen on the side of

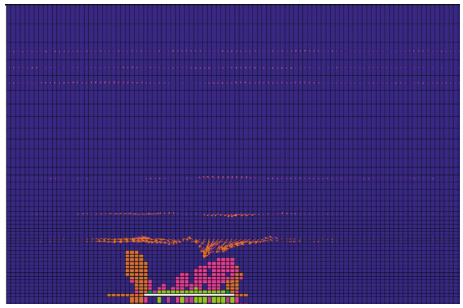

Figure 17: Flow vector diagram when the working face had advanced 100 m.

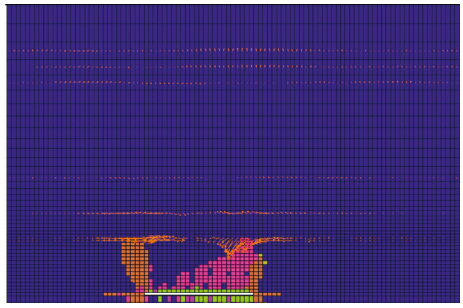

Figure 18: Flow vector diagram when the working face had advanced 120 m.

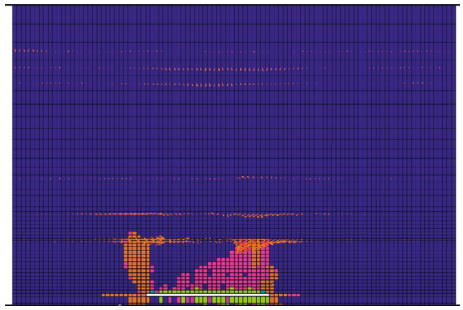

Figure 19: Flow vector diagram when the working face had advanced 140 m.

the terminal mining line on the working face. An observation roadway was excavated from a nearby alley into the overlying stratum, and the appropriate detection profiles were selected to arrange multiple sets of premining comparative holes, along with postmining observation holes. The premining comparative hole A1 and the post-mining observation hole A2 were then taken as a case for introducing the observational results, as shown in Figures 21 and 22. The unit-length seepage of hole A1 was determined to be generally between 0 and 2.5 L/min, which indicated that the original fractures of the rock were insufficiently developed. The water conductivity test of the A2 borehole has found that the seepage of hole A2 was found to be larger at the hole depths between 8 and 43 m within the range of the fractured zone, of which the water-conductive channel reached the upper limitation to the hole at a depth of 43.0 m. The height of the relative mining coal seam in the observation station was 24 m, and the inclination of A2 hole was 18°. Therefore, the height of the water-flowing fractured zone which was calculated using hole A2 was as follows:

$$H_{A2} = 24 + 43.0 \times \sin 18^{\circ} = 37.3\ \text{m}. \quad (9)$$

In this study, through the use of a° comprehensive analysis, it was confirmed that the stress reduction zone and failure field of the overlying strata in the numerical simulation results were consistent with the water-flowing fractured zone in morphology and height, respectively, which presented a certain reliability.

Then, by combining the above test results of all the observation holes, it was concluded that the height of the water-flowing fractured zone was 38 m for the overlying strata on the working face of the coal mine examined in this study.

According to observed results, the development pattern of the water-flowing fractured zone on the first mining face in the Beizao Sea was saddle-shaped, as shown in Figure 23. The lateral propagation (convex) width of the water-flowing fractured zone is determined to be approximately 10 m.

The upper interface of the water-flowing fractured zone was located in the mudstone at the fifth layer of the overlying strata in $coal_2$, with a thickness of 3.9 m. As detailed in the right section of Figure 23, it was a comprehensive stratigraphic column. Therefore, the calculations of the layer thickness and height may have experienced errors. Generally speaking, a water-flowing fractured zone should be terminated in the rock level. It was believed from this study's analysis that the upper interface of the water-flowing fractured zone should have been located at the interface between the mudstone with a thickness of 3.9 m and the carbonaceous mudstone with a thickness of 2.9 m.

The reasons for the formations of a saddle shape and convex lateral boundary of the water-flowing fractured zone are detailed below. At the mining boundary, the curvature of the overlying strata with bending deformation was the largest, and therefore, the height of the mining boundary was the maximum. On the outer side of the mining boundary (above the coal pillar), the overlying stratum with bending deformation was in a tensile stress state, which was prone to open the fractures. Therefore, the lateral boundary of the water-flowing fractured zone was convex.

6. Discussion

In this study, field measurements were conducted on the height range of the water-flowing fractured zone on the roof of the mine. A mechanical structure model was established for theoretically analyzing the failure laws of the "three zones" of the roof under the conditions of the mining processes. A numerical simulation method was adopted to simulate the roof seepage situation during the process of the working face advancement. The numerical simulation results were found to be consistent with the field measurements. Therefore, this numerical modeling method was

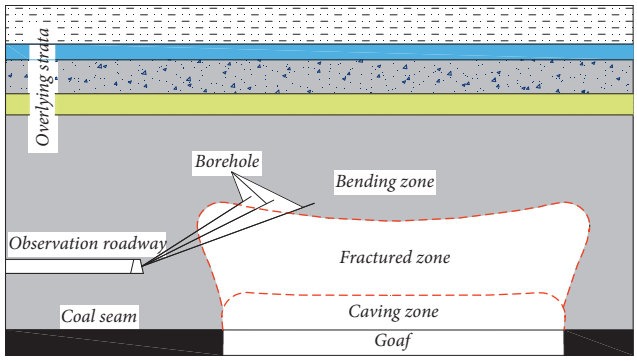

Figure 20: Schematic diagram of height observation of water-flowing fractured zone.

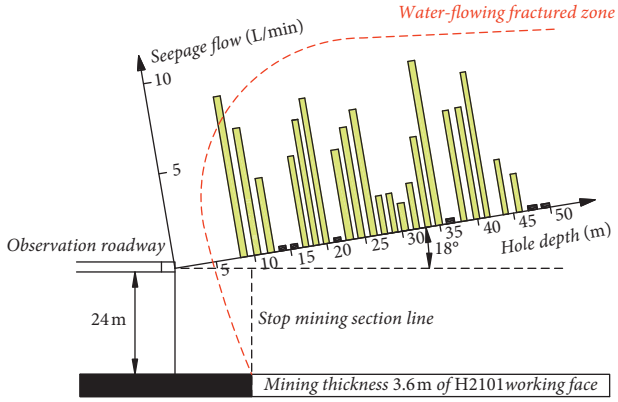

Figure 22: Observed results of postmining hole A2.

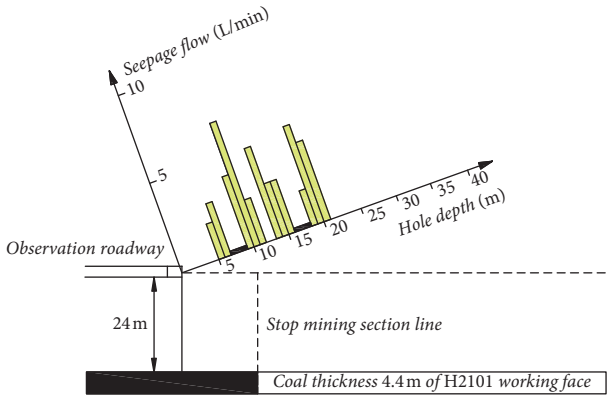

Figure 21: Observed results of premining hole A1.

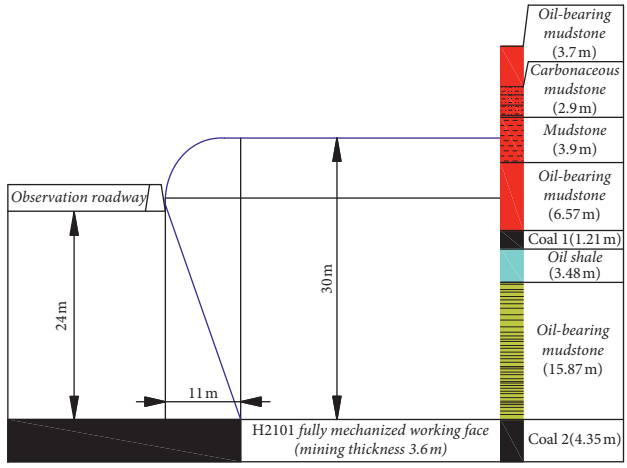

Figure 23: Development morphology of the water-flowing fractured zone on the H2101 plane.

determined to potentially provide a reference for mining under large bodies of water in similar conditions.

7. Conclusions

The conclusions reached in this study were as follows:

(i) As viewed from the numerical calculation analysis and field observations of a coal seam in the Beizao Sea, during the process of the working face advancement, the bed separation mainly occurred in the layers with different mechanical strengths. As the working face advanced, the distribution area of the slow subsidence zone, which was formed by the overlying strata caving and fracture connections, was observed to gradually increase, similar to the affected overlying rock height. However, the caving and breaking rock expansion supported the overlying stratum, and the height of the water-flowing fractured zone connected in the overlying stratum did not always increase and finally stabilized at approximately 38 m. Also, a closure phenomenon occurred which had connected the fractures. It was observed that, above the coal pillar outside the mining boundary, the overlying strata with bending deformation were in a tensile stress state and were prone to open the fractures and convex lateral boundary of the water-flowing fractured zone.

(ii) During the process of coal seam mining, compression-shear and tension-shear tend to lead to the mining fractured zone mainly being concentrated in the stratum above the working face. Therefore, open-off cutting and the mining of the working face are the key factors of the water inrushes in the stratum. The conditions of the water damages are the formation of water inrush channels. The channels for potential water inrushes during underwater mining mainly refer to the water-flowing fractured zones formed by the excavations. In this study, systematical examination were made in regard to the criteria and evolution laws of the fracture propagation for overlying strata in mining fields. The conclusions can be applied to such projects as the comprehensive treatment of water inrushes in the working faces of coal mines.

Data Availability

The data used to support the findings of this study are included within the article.

Conflicts of Interest

The authors declare that there are no conflicts of interest regarding the publication of this paper.

Acknowledgments

The authors would like to acknowledge the support of the State Key Research Development Program of China (no. 2016YFC0600708), the Shandong Provincial Natural Science Foundation (no. ZR2018MEE001), the State Key Laboratory of Open Funds (nos. MDPC201601 and MDPC201703), the Tai'shan Scholar Engineering Construction Fund of Shandong Province of China, and the Tai'shan Scholar Talent Team Support Plan for Advanced and Unique Discipline Areas.

References

[1] A. Gandhe, V. Venkateswarlu, and R. N. Gupta, "Extraction of coal under a surface water body-a strata control investigation," *Rock Mechanics & Rock Engineering*, vol. 38, no. 5, pp. 399–410, 2005.

[2] X. Wu, Q. Yu, X. Wang et al., "Exploitation of coal resources under surface water body," *Chinese Journal of Rock Mechanics and Engineering*, vol. 25, no. 5, pp. 1029–1036, 2006.

[3] Q. Wu, F. Cui, S. Zhao et al., "Type classification and main characteristics of mine water disasters," *Journal of China Coal Society*, vol. 38, no. 4, pp. 561–565, 2013.

[4] X. Miao, C. Wang, and H. Bai, "Hydrogeologic characteristics of mine water hazards in Shendong mining area," *Journal of Mining and Safety Engineering*, vol. 27, no. 3, pp. 285–298, 2010.

[5] W. Qiao, L. Wen-Ping, and L. Xiao-Qin, "Mechanism of "hydrostatic water-inrush" and countermeasures for water inrush in roof bed separation of a mining face," *Journal of Mining and Safety Engineering*, vol. 28, no. 1, pp. 96–104, 2011.

[6] L. Shi, H. Xin, and P. Zhai, "Calculating the height of water flowing fracture zone in deep mining," *Journal of China University of Mining and Technology*, vol. 41, no. 1, pp. 37–41, 2012.

[7] X. Miao, X. Cui, J. Wang, and J. Xu, "The height of fractured water-conducting zone in undermined rock strata," *Engineering Geology*, vol. 120, no. 1–4, pp. 32–39, 2011.

[8] Z. Wen, Y. Tan, Z. Han, and F. Meng, "Construction of time-space structure model of deep stope and stability analysis," *Polish Jouranl of Environmental Studies*, vol. 25, no. 6, pp. 2633–2639, 2016.

[9] V. Palchik, "Formation of fractured zones in overburden due to longwall mining," *Environmental Geology*, vol. 44, no. 1, pp. 28–38, 2003.

[10] R. Chen, H. Bai, and F. Meimei, "Determination of the height of water flowing fractured zone in overburden strata above fully-mechanized top-coal caving face," *Journal of Mining & Safety Engineering*, vol. 23, no. 2, pp. 220–223, 2006.

[11] J. Zhang and B. Shen, "Coal mining under aquifers in China: a case study," *International Journal of Rock Mechanics and Mining Sciences*, vol. 41, no. 4, pp. 629–639, 2004.

[12] Y. Wang and W. Shen, *Prevention and Treatment of the Water Disaster of Coal Mine in China*, China Coal Industry Publishing House, Beijing, China, 1996.

[13] *State Bureau of Coal Industry. Buildings, Water, Railway and Main Shaft and This Coal Pillar and Press Coal Mining Regulations*, China Coal Industry Publishing House, Beijing, China, 2000.

[14] H. Chen, X. Li, A. Liu et al., "Physical simulation modeling of roof water inrush in underwater mining," *Journal of China University of Mining & Technology*, vol. 39, no. 6, pp. 854–859, 2010.

[15] X. Lai, M. Cai, F. Ren, M. Xie, and T. Esaki, "Assessment of rock mass characteristics and the excavation disturbed zone in the Lingxin coal mine beneath the Xitian river, China," *International Journal of Rock Mechanics and Mining Sciences*, vol. 43, no. 4, pp. 572–581, 2006.

[16] S. Peng and J. Wang, *Safety Coal Mining above the Confined Aquifer*, China Coal Industry Publishing House, Beijing, China, 2001.

[17] W. Guo, W. Liu, and W. Zhang, *Special Mining of Mine*, Coal Industry Press, Beijing, China, 2008.

[18] X. Feng and W. Ding, "Meso-mechanical experiment of microfracturing process of rock under coupled mechanical-hydrological-chemical environment," *Chinese Journal of Rock Mechanics and Engineering*, vol. 24, no. 9, pp. 1465–1473, 2005.

[19] Q. Liu and X. Liu, "Research on critical problem for fracture network propagation and evolution with multifield coupling of fractured rock mass," *Rock and Soil Mechanics*, vol. 35, no. 2, pp. 305–320, 2014.

[20] S. Wang, X. Ge, and G. Zhang, "Numerical analysis of crack propagation under compression," *Chinese Journal of Rock Mechanics and Engineering*, vol. 18, no. 6, pp. 671–675, 1999.

[21] S. Li, S. Li, W. Zhu et al., "CT real-time testing study on effect of water on crack growth in fractured rock mass," *Chinese Journal of Rock Mechanics and Engineering*, vol. 23, no. 11, pp. 3584–3590, 2004.

[22] M. D. Zoback, F. Rummel, R. Jung et al., "Laboratory hydraulic fracturing experiments in intact and prefractured rock," *International Journal of Rock Mechanics and Mining Sciences & Geomechanics Abstracts*, vol. 14, no. 2, pp. 49–58, 1977.

[23] C. Wang and B. Xing, "A new theory and application progress of the modified hydraulic test on pre-existing fracture to determine in-situ stresses," *Rock and Soil Mechanics*, vol. 38, no. 5, pp. 1289–1297, 2017.

[24] S. Yang, "Crack coalescence behavior of brittle sandstone samples containing two coplanar fissures in the process of deformation failure," *Engineering Fracture Mechanics*, vol. 78, no. 17, pp. 3059–3081, 2011.

[25] X. Feng, W. Ding, and D. Zhang, "Multi-crack interaction in limestone subject to stress and flow of chemical solutions," *International Journal of Rock Mechanics and Mining Sciences*, vol. 46, no. 1, pp. 159–171, 2009.

[26] T. M. Fayyad and J. M. Lees, "Experimental investigation of crack propagation and crack branching in lightly reinforced concrete beams using digital image correlation," *Engineering Fracture Mechanics*, vol. 182, pp. 487–505, 2017.

[27] C. Li, L. Wang, and X. Wang, "Crack and crack growth behavior analysis of asphalt mixtures based on the digital speckle correlation method," *Engineering Fracture Mechanics*, vol. 147, pp. 487–505, 2017.

[28] S. Yu and F. Xiqiao, *Damage Mechanics*, Tsinghua University Press, Beijing, China, 1997.

[29] Itasca Consulting Group, Inc., *Fast Language Analysis of Continua in 3 Dimensions (version 5.0)*, Itasca Consulting Group, Inc., Minneapolis, MN, USA, 2012.
[30] X. Miao, W. Liu, and Z. Chen, *Seepage theory of mining rock mass*, Science Press, Beijing, China, 2004.
[31] L. Li, S. Li, S. Shi et al., "Water inrush mechanism study of fault activation induced by coupling effect of stress-seepage-damage," *Chinese Journal of Rock Mechanics and Engineering*, no. s1, pp. 3295–3304, 2011.
[32] J. Zhang, "Investigations of water inrushes from aquifers under coal seams," *International Journal of Rock Mechanics and Mining Sciences*, vol. 42, no. 3, pp. 350–360, 2005.
[33] M. Xie and M. Qian, "Advance in the key strata theory of mining rockmass," *Journal of China University of Mining and Technology*, vol. 29, no. 1, pp. 25–29, 2000.
[34] L. Wang, Z. Wang, J. Huang et al., "Prediction on the height of water-flowing fractured zone for shallow seam covered with thin bedrock and thick windblown sands," *Journal of Mining and Safety Engineering*, vol. 29, no. 5, pp. 607–612, 2012.
[35] S. S. Peng, *Surface Subsidence Engineering*, Society for Mining, Metallurgy and Exploration, Englewood, CO, USA, 1992.
[36] J. Xu, W. Zhu, and X. Wang, "New method to predict the height of fractured water-conducting zone by location of key strata," *Journal of China Coal Society*, vol. 37, no. 5, pp. 762–769, 2012.
[37] Y. Gao, Z. Qu, F. Xing et al., "Observation of height of excavating face H2106 in Longkoubeizao mine under sea," *Coal Geology and Exploration*, vol. 37, no. 6, pp. 35–38, 2009.